Polymer Chemistry

ROYAL SOCIETY OF CHEMISTRY

PAPER

View Article Online
View Journal | View Issue

Cite this: *Polym. Chem.*, 2022, **13**, 2307

Nonionic nontoxic antimicrobial polymers: indole-grafted poly(vinyl alcohol) with pendant alkyl or ether groups†

Xiaoya Li,[a] Sedef İlk,[b,c] Yang Liu,[d] Deepak Bushan Raina,[d] Deniz Demircan[a] and Baozhong Zhang *[a]

A series of new nonionic antimicrobial polymers with a biodegradable polyvinyl alcohol (PVA) backbone grafted with indole units and different hydrophobic alkyl or ether groups were synthesized by facile esterification. The chemical structures and thermal properties of the obtained polymers were characterized by GPC, NMR, FTIR, WAXD, TGA and DSC analyses. All these nonionic polymers showed a significant antibacterial effect similar to gentamicin against 9 food and human pathogenic bacteria according to the disk diffusion assay. The presence of alkyl or ether groups in most cases did not significantly affect the antibacterial effect compared to the polymer with unsubstituted indole units (with N–H moieties). The impacts of the OH conversion and molecular weight of the obtained polymers on their antimicrobial and anti-quorum sensing effects were also preliminarily investigated. Finally, the obtained indole-grafted PVAs were subjected to MTT assay using a mammalian cell line and hemolysis investigations, and the results showed excellent biocompatibility, particularly for those with ether substituents.

Received 8th November 2021,
Accepted 20th March 2022

DOI: 10.1039/d1py01504d

rsc.li/polymers

Introduction

Antimicrobial polymers (APs) have been under rapid development in the past decade, due to their enhanced antimicrobial activity,[1–3] low potential to induce antimicrobial resistance,[4–9] and low leaching risk and environmental toxicity compared to small molecular antimicrobials.[10–15] Currently most reported APs are ionic, and their ionic interactions with bacterial membranes are essential for their antimicrobial function.[16–22] However, for certain applications, ionic polymers may suffer from undesirable water solubility, fouling risk and toxicity.[23–28] Therefore, new APs without ions have become an attractive target with high potential.[29,30]

Nonionic polymers do not have ionic interactions with bacteria, so they should be endowed with the ability to interact with bacteria by other grafted nonionic biologically active units, such as glucose, curcumin, astaxanthin, tropolone, aspirin, limonene, indole, isatin, anisole, *etc.*[31–39] These biologically active molecules are known for their ability to interact with bacteria, and they have been adapted by the natural ecosystem and thus tend to be more biodegradable and less eco-toxic.[40,41] Some of these biologically active molecules (*e.g.* limonene, indole, and aspirin) also show anti-quorum sensing effects.[37,42,43] Grafting these molecules onto a polymer backbone could enable interactions between the polymers and bacterial membranes leading to an antimicrobial effect.[29,44–51] Such nonionic interactions can be complex, including hydrogen bonding, hydrophobic, dipole, and aromatic interactions.[10,52–55] However, the general mechanism related to the antimicrobial function of nonionic APs remains to be unravelled.

Indole is a bio-sourced nonionic building block that is ubiquitous in nature and domestic wastes,[56,57] and it has received growing attention for the development of bio-based polymers toward various high performance packaging and textile applications.[58–61] In the meantime, many indole derivatives are natural antibiotics,[31,62,63] and several indole-based polyesters, polyketones and polyurethanes have been reported with antibacterial effects.[44,64,65] Indole groups can also have a synergistic antibacterial effect when grafted on polymers

[a]*Lund University, Centre for Analysis and Synthesis, Department of Chemistry, P. O. Box 124, SE-22100 Lund, Sweden. E-mail: baozhong.zhang@chem.lu.se*
[b]*Niğde Ömer Halisdemir University, Faculty of Medicine, Department of Immunology, TR-51240 Niğde, Turkey*
[c]*KTH Royal Institute of Technology, School of Engineering Sciences in Chemistry, Biotechnology and Health, Department of Chemistry, Division of Glycoscience, SE-10691 Stockholm, Sweden*
[d]*Faculty of Medicine, Department of Clinical Sciences, Orthopedics, Lund University, Lund, Sweden*

†Electronic supplementary information (ESI) available: Synthesis scheme of grafting agents **2–6**; analytical data of grafting agents **1–6** (^{1}H NMR and ^{13}C NMR spectra); zoomed-in ^{1}H NMR spectra of PVA; calculations of OH conversion of **PI1–6**; analytical data of **PI1–6** (solubility data, ^{13}C NMR, GPC and UV-vis spectra); WAXD spectra of PVA and **PI1–6**; inhibition zones of **PI1–6**; *p* values of the antimicrobial results; analytical data of $\mathbf{PI4}_{54}$, $\mathbf{PI4}_{72}$ and $\mathbf{PI4}_{85}$ (^{1}H NMR spectra and GPC spectra); plates of disk diffusion tests and anti-QS tests of $\mathbf{PI4}_{54}$, $\mathbf{PI4}_{72}$ and $\mathbf{PI4}_{85}$; UV absorbance at 600 nm of **PI1** in MTT assay. See DOI: https://doi.org/10.1039/d1py01504d

together with other antibacterial moieties (*e.g.* metal ions, ammonium cations, chitosan, and aldehyde).[66–69] In addition, indole-based APs can also have desirable miscibility with other matrix polymers so they are potentially suitable antimicrobial additives.[30]

Despite the promising potential of indole-based nonionic APs, the knowledge regarding the role of indole units and other structural factors in their antimicrobial function remains rather limited. For instance, hydrophobic substituents (*e.g.* alkyl or ether groups and aromatic units) frequently enhance the antimicrobial effect of ionic APs,[70,71] but it remains unclear whether such an effect exists in nonionic APs. Furthermore, the N–H moiety of indole is a hydrogen bond donor, which can form hydrogen bonds with various hydrogen-accepting groups (*e.g.* ethers or amides in peptidoglycan) in bacterial membranes.[72] It remains to be unraveled whether such hydrogen bond interactions are essential for their antimicrobial effects.[30] Finally, the effects of molecular weights and the hydrophilic/hydrophobic balance of nonionic APs also remained largely unexplored.

In order to shed some light on the roles of indole and other structural factors such as hydrogen bonding or hydrophobic interactions, we herein report on the synthesis of six nonionic indole-based APs with biodegradable poly(vinyl alcohol) backbones, which contain the N–H unit or different linear or cyclic alkyl or ether groups. The molecular structures, thermal properties, antimicrobial effects and cytotoxicity of the obtained nonionic APs were investigated. The impact of hydrophobic *N*-substitution as well as the grafting density and molecular weight on the antimicrobial effects of the obtained nonionic APs was preliminarily evaluated.

Experimental

Chemicals and materials

Poly(vinyl alcohol) (M_w 9000–10 000, 80% hydrolyzed), indole-3-acetic acid, 1-iodopropane, 1-iodohexane, 2-methoxyethyl-4-methylbenzenesulfonate, 1-bromo-2-cyclohexylethane, phenoxyethyl bromide, 1-ethyl-3-(3′-dimethylaminopropyl)-carbodiimide·HCl (EDC–HCl), and 4-dimethylaminopyridine (DMAP) were purchased from Sigma-Aldrich. *N*,*N*-Dimethylformamide (DMF), *N*,*N*-dimethylacetamide (DMAc), dimethyl sulfoxide (DMSO), hydrochloric acid (HCl), sodium hydroxide (NaOH), ethanol, acetone, chloroform, ethyl acetate (EtOAc), diethyl ether, potassium carbonate (K_2CO_3), sodium carbonate (Na_2CO_3), sodium bicarbonate ($NaHCO_3$) (ACS, Reag. Ph. Eur.), and anhydrous sodium sulphate (Na_2SO_4) were purchased from VWR Chemicals. All chemicals were used directly without further purification.

Synthesis

General procedure for *N*-substituted indole-3-acetic acids (2–6). Indole-3-acetic acid **1** (1.75 g, 10.0 mmol, 1.00 eq.) was dissolved in anhydrous DMF (10 mL) and cooled on an ice bath with stirring. A solution of NaH (1.00 g, 25.0 mmol, 2.50 eq.) in DMF (10 mL) was added dropwise and the resulting dark coloured suspension was stirred at rt for 1 h. The grafting agent (*i.e.* 1-iodopropane, 1-iodohexane, 1-bromo-2-cyclohexylethane, 2-methoxyethyl-4-methylbenzene-sulfonate, or phenoxyethyl bromide) was added (11.0 mmol, 1.10 eq.), and the reaction mixture was stirred at rt for 18 h. Afterward, the reaction mixture was diluted with water (50 mL) and conc. HCl dropwise, followed by extraction with EtOAc (3 × 50 mL). The combined organic phase was washed with water and brine, dried over anhydrous Na_2SO_4, and concentrated *in vacuo*, yielding a solid product (**2–6**), which was dried at 50 °C under vacuum for 12 h until a constant weight was reached.

*N-Propyl-3-indoleacetic acid (**2**).* Yield 90%; brown powder. ^{1}H NMR (400.13 MHz, DMSO-d_6) δ, ppm: δ 12.20 (s, 1H), 7.52 (d, 1H), 7.43 (d, 1H), 7.27 (s, 1H), 7.13 (t, 1H), 7.02 (t, 1H), 4.08 (t, 2H), 3.65 (s, 2H), 1.75 (m, 2H), 0.84 (t, 3H). ^{13}C NMR (100.61 MHz, DMSO-d_6) δ, ppm: 173.50, 136.39, 128.07, 127.72, 121.48, 119.36, 118.92, 110.16, 107.45, 47.35, 31.40, 23.67, 11.66. UV (DMF): λ_{max} 288 nm (ε 3.73 × 10^3 M^{-1} cm^{-1}). FTIR: ν = 2960, 1709, 1471, 1391, 1231, 1205, 1188, 910, 805, 730 and 654 cm^{-1}. HRMS (ESI+, *m*/*z*): exact mass calcd for $C_{13}H_{16}NO_2^+$, 218.1181; found, 218.1180.

*N-Hexyl-3-indoleacetic acid (**3**).* Yield 94%; brown powder. ^{1}H NMR (400.13 MHz, DMSO-d_6) δ, ppm: ^{1}H NMR (400.13 MHz, DMSO-d_6) δ, ppm: δ 12.20 (s, 1H), 7.52 (d, 1H), 7.42 (d, 1H), 7.26 (s, 1H), 7.13 (t, 1H), 7.02 (t, 1H), 4.11 (t, 2H), 3.65 (s, 2H), 1.72 (m, 2H), 1.26 (m, 6H), 0.84 (t, 3H). ^{13}C NMR (100.61 MHz, DMSO-d_6) δ, ppm: 173.51, 136.31, 128.03, 127.66, 121.48, 119.35, 118.88, 110.07, 107.45, 45.75, 31.31, 30.33, 26.42, 22.48, 14.32. UV (DMF): λ_{max} 290 nm (ε 3.79 × 10^3 M^{-1} cm^{-1}). FTIR: ν = 2929, 1702, 1471, 1369, 1230, 1213, 939, 785, 725 and 645 cm^{-1}. HRMS (ESI+, *m*/*z*): exact mass calcd for $C_{16}H_{22}NO_2^+$, 260.1651; found, 260.1650.

*N-(2-Cyclohexylethyl)-3-indoleacetic acid (**4**).* Yield 75%; brown powder. ^{1}H NMR (400.13 MHz, DMSO-d_6) δ, ppm: δ 12.20 (s, 1H), 7.50 (d, 1H), 7.40 (d, 1H), 7.26 (s, 1H), 7.12 (t, 1H), 7.01 (t, 1H), 4.14 (t, 2H), 3.63 (s, 2H), 1.75 (m, 2H), 1.63 (m, 5H), 1.17 (m, 4H), 0.95 (m, 2H). ^{13}C NMR (100.61 MHz, DMSO-d_6) δ, ppm: 173.52, 136.20, 128.07, 127.55, 121.51, 119.38, 118.90, 110.00, 107.52, 43.61, 37.76, 35.10, 33.03, 31.31, 26.52, 26.15. UV (DMF): λ_{max} 292 nm (ε 3.74 × 10^3 M^{-1} cm^{-1}). FTIR: ν = 2921, 1696, 1469, 1306, 1138, 1013, 960, 795, 735 and 644 cm^{-1}. HRMS (ESI+, *m*/*z*): exact mass calcd for $C_{18}H_{24}NO_2^+$, 286.1807; found, 286.1801.

*N-Methoxyethyl-3-indoleacetic acid (**5**).* Yield 68%; brown powder. ^{1}H NMR (400.13 MHz, DMSO-d_6) δ, ppm: δ 12.20 (s, 1H), 7.50 (d, 1H), 7.45 (d, 1H), 7.25 (s, 1H), 7.13 (t, 1H), 7.02 (t, 1H), 4.29 (t, 2H), 3.64 (m, 4H), 3.22 (t, 3H). ^{13}C NMR (100.61 MHz, DMSO-d_6) δ, ppm: 173.50, 136.54, 128.04, 128.03, 121.53, 119.28, 119.00, 110.23, 107.58, 71.58, 58.52, 45.62, 31.30. UV (DMF): λ_{max} 288 nm (ε 4.15 × 10^3 M^{-1} cm^{-1}). FTIR: ν = 2882, 1694, 1469, 1303, 1115, 1011, 947, 833, 736 and 647 cm^{-1}. HRMS (ESI+, *m*/*z*): exact mass calcd for $C_{13}H_{16}NO_3^+$, 234.1130; found, 234.1126.

*N-(2-Phenyloxylethyl)-3-indoleacetic acid (**6**).* Yield 72%; brown powder. ^{1}H NMR (400.13 MHz, DMSO-d_6) δ, ppm:

δ 12.20 (s, 1H), 7.56–6.86 (m, 10H), 4.54 (t, 2H), 4.27 (t, 2H), 3.65 (s, 2H). ^{13}C NMR (100.61 MHz, DMSO-d_6) δ, ppm: 173.48, 158.54, 136.63, 129.97, 128.10, 128.09, 121.65, 121.29, 119.15, 114.93, 110.35, 107.89, 67.37, 45.35, 31.29. UV (DMF): λ_{max} 288 nm (ε 3.83 × 10^3 M^{-1} cm^{-1}). FTIR: ν = 2921, 1702, 1594, 1499, 1464, 1232, 1206, 1054, 903, 782, 753, 734, 688 and 654 cm^{-1}. HRMS (ESI+, *m*/*z*): exact mass calcd for $C_{18}H_{18}NO_3^+$, 296.1287; found, 296.1285.

General synthetic procedure for indole-based PVAs (PI1–6). A solution of **PVA** (0.100 g, 1.86 mmol OH groups), **1–6** (1.86 mmol, 1.00 eq. with respect to OH groups), EDC–HCl (0.390 g, 2.10 mmol, 1.10 eq.) and DMAP (0.01 g, 5 wt%) in DMF (5 mL) in a capped 25 mL round-bottom flask was stirred at rt for 24 h. Afterward, the reaction mixture was added into a saturated $NaHCO_3$ solution (200 mL). The resulting brown precipitates were collected and dissolved in 2 mL of DMF (for **PI1–2** and **PI4–6**) or acetone (for **PI3**) and re-precipitated from 100 mL of diethyl ether. The resulting precipitates were re-dissolved in 2 mL of DMF and precipitated from 200 mL of water. The precipitates were collected by gravity filtration and dried at 50 °C under vacuum for 24 h to yield a brown solid (**PI1–6**).

PI1. Yield 45%; brown powder. ^{1}H-NMR (400 MHz, DMSO-d_6) δ, ppm: 10.90 (s, 1H, NH), 7.50 (s, 1H, Ar), 7.34 (s, 1H, Ar), 7.22 (s, 1H, Ar), 7.06 (s, 1H, Ar), 6.98 (s, 1H, Ar), 5.24–4.75 (m, C*H*OOR) 4.75–4.18 (m, O*H*), 3.96–3.78 (m, C*H*OH), 3.77–3.57 (m, 2H, ArCH_2COOR), 2.04–1.86 (m, CH_3COOR), 1.86–1.13 (m, $R_1CH_2R_2$). ^{13}C NMR (100.61 MHz, DMSO-d_6) δ, ppm: 171.40, 170.19, 136.53, 127.60, 124.42, 121.51, 118.95, 117.82, 107.65, 68.72–63.43, 47.12–44.63, 31.30, 21.24. FTIR: ν = 3411, 2925, 1720, 1458, 1371, 1245 and 742 cm^{-1}.

PI2. Yield 40%; brown powder. ^{1}H-NMR (400.13 MHz, DMSO-d_6) δ, ppm: 7.60–6.79 (m, 5H, Ar), 5.35–4.74 (m, C*H*OOR) 4.74–4.18 (m, O*H*), 4.16–3.90 (m, N$CH_2$$CH_2$CH), 3.86–3.75 (m, C*H*OH), 3.75–3.54 (m, 2H, ArCH_2COOR), 2.04–1.84 (m, CH_3COOR), 1.84–1.13 (m, NCH$_2$$CH_2CH_3$, $R_1CH_2R_2$), 0.92–0.59 (m, NCH$_2$CH$_2$$CH_3$). ^{13}C NMR (100.61 MHz, DMSO-d_6) δ, ppm: 171.45, 170.34, 136.32, 127.96, 127.68, 121.52, 119.28, 118.95, 110.09, 106.66, 70.63–62.89, 47.33, 46.35–44.57, 31.13, 23.59, 21.17, 11.61. FTIR: ν = 3422, 2929, 1729, 1468, 1370, 1243 and 740 cm^{-1}.

PI3. Yield 28%; brown powder. ^{1}H-NMR (400.13 MHz, DMSO-d_6) δ, ppm: 7.62–6.85 (m, 5H, Ar), 5.32–4.74 (m, C*H*OOR) 4.74–4.22 (m, O*H*), 4.18–3.52 (m, N$CH_2$$(CH_2)_4CH_3$, C*H*OH, ArC$H_2$COOR), 2.02–1.84 (m, C$H_3$COOR), 1.84–1.02 (m, NCH$_2$$(CH_2)_4CH_3$, $R_1CH_2R_2$), 0.88–0.65 (m, CH$_2$$CH_3$). ^{13}C NMR (100.61 MHz, DMSO-d_6) δ, ppm: 171.53, 170.14, 136.28, 127.94, 127.64, 121.54, 119.32, 118.95, 110.04, 106.87, 68.42–63.68, 45.82, 46.93–44.59, 31.32, 30.30, 26.42, 22.52, 21.27, 14.30. FTIR: ν = 3426, 2929, 1729, 1468, 1370, 1240 and 738 cm^{-1}.

PI4. Yield 35%; brown powder. ^{1}H-NMR (400.13 MHz, DMSO-d_6) δ, ppm: 7.84–6.83 (m, 5H, Ar), 5.30–4.75 (m, CHOOR) 4.75–4.17 (m, OH), 4.17–3.54 (m, NCH_2CH$_2$$(CH_2)_6$, *CH*OH, Ar$CH_2$COOR), 2.08–1.84 (m, CH_3COOR), 1.84–0.28 (m, N CH$_2$$CH_2$$(CH_2)_6$, $R_1CH_2R_2$). ^{13}C NMR (100.61 MHz, DMSO-d_6) δ, ppm: 171.45, 170.15, 136.14, 127.98, 127.43, 121.52, 119.31, 118.93, 109.90, 106.83, 71.04–63.36, 47.32–44.47, 43.61, 37.69, 35.04, 32.97, 31.15, 26.47, 26.10, 21.21. FTIR: ν = 3442, 2921, 1732, 1468, 1370, 1243 and 736 cm^{-1}.

PI5. Yield 23%; brown powder. ^{1}H-NMR (400.13 MHz, DMSO-d_6) δ, ppm: 7.58–6.83(m, 5H, Ar), 5.35–4.73 (m, CHOOR), 4.73–4.01 (m, OH, NCH_2CH$_2$OCH$_3$), 4.01–3.45 (m, C*H*OH, ArCH_2COOR, NCH$_2$$CH_2OCH_3$), 3.27–3.06 (NCH$_2CH_2OCH_3$), 2.08–1.86 (m, C$H_3$COOR), 1.86–1.18 (m, $R_1CH_2R_2$). ^{13}C NMR (100.61 MHz, DMSO-d_6) δ, ppm: 171.61, 170.42, 136.60, 128.05, 127.96, 121.59, 119.26, 119.08, 110.23, 107.08, 71.57, 68.69–63.42, 58.52, 46.53–44.42, 45.67, 31.18, 21.25. FTIR: ν = 3434, 2929, 1729, 1468, 1370, 1243 and 740 cm^{-1}.

PI6. Yield 30%; brown powder. ^{1}H-NMR (400.13 MHz, DMSO-d_6) δ, ppm: 7.63–6.65 (m, 10H, Ar), 5.36–4.75 (m, C*H*OOR) 4.75–3.98 (m, O*H*, N$CH_2$$CH_2$O), 3.98–3.54 (m, C*H*OH, ArCH_2COOR), 2.03–1.83 (m, CH_3COOR), 1.83–0.98 (m, $R_1CH_2R_2$). ^{13}C NMR (100.61 MHz, DMSO-d_6) δ, ppm: δ, ppm: 171.44, 170.18, 136.61, 129.93, 128.02, 121.70, 121.46, 121.24, 119.23, 114.86, 110.34, 107.37, 67.66–62.91, 67.45, 46.79–44.52, 45.35, 31.15, 21.21. FTIR: ν = 3438, 2925, 1731, 1598, 1494, 1468, 1373, 1241, 742 and 692 cm^{-1}.

Measurements

Nuclear magnetic resonance (NMR) spectra were recorded on a Bruker DRX400 spectrometer at a proton frequency of 400.13 MHz and a carbon frequency of 100.61 MHz. Fourier transform infrared (FT-IR) spectra were obtained with an attenuated total reflection (ATR) setup using a Bruker Alpha FT-IR spectrometer. Differential scanning calorimetry (DSC) measurements were performed using a TA Instruments DSC Q2000. The samples were studied at a heating rate of 10 °C min^{-1} under nitrogen with a purge rate of 50 mL min^{-1}. The T_g value was taken as the midpoint of the endothermic step-change observed during the second heating run. Thermogravimetric analysis (TGA) was performed under a nitrogen atmosphere with a Thermogravimetric Analyzer (TA Instrument Q500) at a heating rate 10 °C min^{-1}. Gel permeation chromatography (GPC) was carried out with three Shodex columns in series (KF-805, 2804, and 2802.5) and a refractive index (RI) detector (Viscotek Model 250). All measurements were carried out at room temperature at a concentration of 30 mg mL^{-1} using chloroform as the eluent, and at an elution rate of 1 mL min^{-1}. Calibration was performed with four polystyrene standard samples (M_n = 650 kg mol^{-1} from Water Associates, 96 and 30 kg mol^{-1} from Polymer Laboratories, and 3180 g mol^{-1} from Agilent Technologies). UV-visible spectra were recorded with an UV-visible spectrometer in the wavelength range from 200 to 600 nm with a resolution of 2 nm, employing quartz cuvettes of 10 mm path length. WXRD (wide angle X-ray diffraction) diffraction patterns were recorded with a Stoe Stadi MP X-ray powder diffractometer in the transmission mode over 2θ ranges 2–60° with Cu Kα radiation. High resolution mass spectrometry (HRMS) was performed by direct infusion on a Water Xevo-G2 QTOF mass spectrometer using electrospray ionization.

Antimicrobial bioassay

Bacterial culture. Microorganisms *Escherichia coli* ATCC 25922 (*Ec*), *Staphylococcus aureus* ATCC 25923 (*Sa*), *Proteus mirabilis* ATCC 14153 (*Pm*), *Proteus vulgaris* ATCC13315 (*Pv*), *Pseudomonas aeruginosa* ATCC 27853 (*Pa*), *Enterobacter aerogenes* ATCC13048 (*Ea*), *Bacillus thuringiensis* (*Bt*), *Salmonella typhimurium* SL1344 (*St*) and *Streptococcus mutans* ATCC 25175 (*Sm*) were employed to evaluate the antibacterial properties of indole-based PVAs (**PI1–6**). All bacteria strains were sub-cultured on (Luria Bertani) LB agar culture at 37 °C for 24 h.

Disk diffusion assay. Disk-diffusion assay according to the modified standard method was applied to evaluate the antibacterial properties.[35] First, the tested solid samples (indole-based PVAs) were dissolved in DMF (10 μg mL^{-1}, w/v). Microorganisms' susceptibility was adjusted with 0.5 McFarland as a reference standard. The prepared solutions were sterilized under UV light for 5 min before test. Microorganism culture suspension (100 μL, 10^6 cells per mL) was swabbed onto a plate within Müller-Hinton agar. Sterile disks with a diameter of 6 mm were placed on the Petri plate inoculated with microorganisms, and 20 μL of the prepared sample solutions were loaded on the disks. Afterward, bacteria cultures were incubated at 37 °C for 24 h. Disks containing gentamicin (10 μg per disk) or DMF (pure solvent) were used as a positive or negative control, respectively. All experiments were performed in triplicate (*i.e.* 3 biological replicates with 3 technical repeats for each tested bacteria strain). The results are expressed as the mean diameter of the inhibition zone in mm ± standard deviation (mean ± SD). Significant differences between two groups were evaluated as p values by t-test using Microsoft Excel software. $p < 0.05$ indicates significant difference, while $p \geq 0.05$ indicates insignificant difference.

Anti-quorum sensing (anti-QS)

The quorum sensing inhibitory (anti-QS) activity of three **PI4** samples (**$PI4_{54}$**, **$PI4_{72}$**, and **$PI4_{85}$**, 10 μg mL^{-1} in DMF, w/v) was evaluated by the disk diffusion assay against *C. violaceum* CV026 according to the literature procedure.[30,73,74] The bacteria suspension was sub-cultured in LB broth at 30 °C for 24 h. The Petri plates with LB soft agar containing signal molecule *N*-hexanoyl-L-homoserine lactone (C6-HSL, 0.25 μg mL^{-1}) were inoculated with the bacteria culture. Afterward, sterile discs (diameter: 6 mm) loaded with samples (20 μL) were placed on the Petri plates and incubated at 30 °C for 24 h. Gentamicin (10 μg per disc) and the solvent (DMF) were used as positive or negative controls, respectively. The anti-QS activity was evaluated by the turbid halo formation around the disc (in contrast to the purple background).

Minimum inhibitory concentration (MIC) evaluations

The minimum inhibitory concentration (MIC) of the three **PI4** samples (**$PI4_{54}$**, **$PI4_{72}$**, and **$PI4_{85}$**) against two bacteria (*Escherichia coli* ATCC 8739 and *Pseudomonas fluorescens* (PCL 1701)) was determined using the method described in the guideline of *The Clinical and Laboratory Standards Institute*.[75] Briefly, the bacterial suspensions were adjusted using 0.5 McFarland's standard (10^8 CFU mL^{-1}) and the tested polymers were dissolved in DMF. Serial two-fold dilutions of samples' solution (in a 96-well microtiter plate) in concentrations ranging from 100 μg mL^{-1} to 0.19 μg mL^{-1} were used to determine the MIC in the Mueller Hinton broth (MHB). After mixing the samples and MHB, the 96-well microtiter plates were covered with a sterile plate sealer and incubated at 37 °C for 24 h. The only medium was used as the negative control and only bacterial inoculums was used as the positive control. All experiments were performed in triplicate. The MIC value was taken at the lowest concentration of samples where no visible growth is seen in the wells.

Leaching evaluations by UV-vis

Suspensions of **PI1–6** in PBS buffer (100 μg mL^{-1}) were incubated at 37 °C for 24 h with mild magnetic stirring. The UV-vis spectra of their supernatants at the initial point (PIX-initial) and after 24 h (PIX-24 h) were recorded. The UV-vis spectra of **PI1–6** in DMSO (25 μg mL^{-1}) were also recorded as references.

MTT assay

MG-63 cells were purchased from American Type Culture Collection (ATCC) (LOT: 70016786). The MG-63 osteoblast-like human cells were cultured in Dulbecco's Modified Eagle's Medium (DMEM) supplemented with 10% fetal bovine serum (FBS), 1% penicillin, and 1% streptomycin in a humidified incubator at 37 °C. The medium was replaced every 2 days. Cells were trypsinized and centrifuged at 400*g* for 4 min to obtain a concentrated cell pellet when the confluence reached 80%. 1×10^4 cells per well were seeded on a 96-well plate and cultured for 24 h before adding the materials. Test compounds (negative control, **1–6**, and **PI1–6**) dissolved in DMSO were then added to the cell culture at a final DMSO concentration of 1% (v/v), which formed suspensions. Fresh culture medium without samples was used as the negative control, and each sample was replicated in four wells. After being cultured for 24 h, the cell culture medium was discarded and the cells were washed with phosphate buffer once. MTT working solution (0.5 mg mL^{-1}) was added to the cells and incubated for 2 h at 37 °C, after which DMSO (200 μL per well) was added to the reaction products for 10 min. The solubilized contents were pipetted and transferred into a clear bottom 96-well plate. Absorbance was determined by spectrophotometry at 600 nm wavelength. In addition, to evaluate the interaction between **PI1** and MTT working solution, only the material (*i.e.* **PI1**) was subjected to the above procedures under the same conditions without adding the cells.

Hemolysis tests

The HaemoScan Biomaterial Haemolytic Assay (HaemoScan, Netherlands) was used to investigate the cytotoxicity of **PI1–6** on human erythrocytes according to the manufacturer's protocol.[76] The concentrated erythrocytes were included in this kit (LOT: 220307). Briefly, the erythrocyte was prepared by repeatedly rinsing with different wash buffers (dilution buffer I, II

and III, provided by the manufacturer) and centrifuged at 400*g* for 10 minutes. Afterward, 5 mL of dilution buffer III was added to re-suspend the erythrocytes. 0.5 mL of erythrocyte suspension was used to test each sample. **PI1–6** samples were first dissolved in DMSO to form 10 mg mL^{-1} stock solutions. 5 μL of the stock solution was added in 0.5 mL of erythrocyte suspension with a final (suspension) concentration of 100 μg mL^{-1} for polymers. After 24 h of incubation, the samples were centrifuged at 4500*g* for 1 min and 20 μL of the supernatant was pipetted into a 96-well plate along with 180 μL of assay buffer. The absorbance was read at a wavelength of 450 nm. Each polymer was tested in triplicate. DMSO (5 μL, 1% v/v) was used as the negative control (0% hemolysis). Lysis buffer was used as the positive control (100% hemolysis). The hemolysis percentage was calculated using the following equation:

$$\text{Hemolysis}\% = \frac{OD_{450}(\text{sample}) - OD_{450}(\text{negative control})}{OD_{450}(\text{positive control}) - OD_{450}(\text{negative control})} \times 100\%$$

Results and discussion

Synthesis of indole-grafted PVAs

Six indole-grafted PVAs (**PI1–6**) were conveniently synthesized by esterification at room temperature of the **PVA** backbone using the corresponding carboxylic acids (**1–6**) as grafting agents (Scheme 1). Indole carboxylic acid (**1**) is commercially available, while the other five agents (**2–6**) were synthesized by a straightforward S_N2 reaction using **1** and the corresponding electrophilic agents (1-iodopropane, 1-iodohexane, 1-bromo-2-cyclohexylethane, 2-methoxyethyl-4-methylbenzene-sulfonate and phenoxyethyl bromide, Scheme S1, ESI†). The conversion of the OH groups (p_{OH}) on **PVA** backbones after grafting was evaluated using the integrals of the residual OH signals and the aromatic signals in the ^{1}H-NMR spectra (Fig. S3 for **PI1** and Fig. S4 for **PI6** as examples, ESI†). As shown in Table 1, p_{OH} for **PI1–6** was not identical but has a relatively narrow dispersity range (59–72%) considering the accuracy of the quantification method and intrinsic polydispersity of polymers. To obtain some preliminary insight into the possible impacts of the OH conversion, three **PI4** samples with OH conversions of 54%, 72% and 85% were synthesized by using different amounts of grafting agents. Their biological activities were compared in the later session. The resulting crude polymers were purified by precipitation twice to completely remove the unreacted grafting agents and solvents, which causes loss of the products and decreased yields (23–45%). The obtained polymers showed good solubility in polar aprotic solvents (*e.g.* DMF, DMSO, and DMAc) and low solubility in protic solvents (*e.g.* H_2O and ethanol). In addition, the low water solubility of these polymers was further demonstrated by the low UV-vis absorption of the aqueous phase where the polymers were immersed for 24 h (Fig. S10A, ESI†). The same result also indicated that the purification of the polymers was successful without any noticeable small molecular agent left.

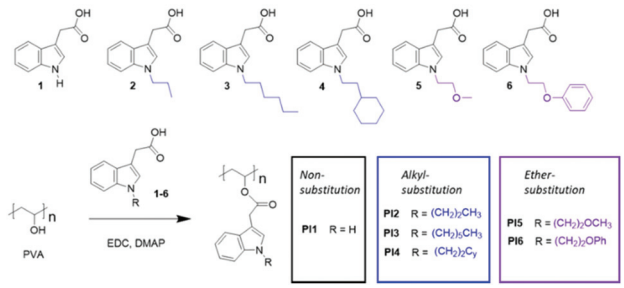

Scheme 1 Synthesis of various indole-grafted PVAs (**PI1–6**), using the corresponding carboxylic acid as grafting agents (**1–6**). Note that the starting **PVA** contains 80% OH and 20% acetate (OAc) groups. The OAc groups remained unchanged after the reaction, which were omitted in the chemical structures.

Molecular and thermal characterization

The chemical structures of the obtained polymers were confirmed by ^{1}H NMR spectroscopy analysis (Fig. 1). The starting polymer **PVA** contains both OH and OAc substituents, as shown in its ^{1}H NMR spectrum (Fig. 1A). The signal at ~1.97 ppm (2) is attributed to the Oac protons. The broad signals at 3.97–3.56 ppm (3) and 5.17–4.73 ppm (5) correspond to the backbone CH groups that are adjacent to the OH and OAc groups, respectively. According to the ratio between the integrals of signals 3 and 5, the initial **PVA** contains ~78% of OH and ~22% of OAc groups, which is consistent with the data from the supplier (80 and 20%). The signals for OH

Table 1 Molecular and thermal properties of **PVA** and **PI1–6**. p_{OH} (conversion of the OH groups) and molecular weight (M_{NMR}) were measured according to ^{1}H NMR data. M_n, M_w and $Đ$ were determined by GPC in chloroform. T_g is the glass transition temperature measured by DSC second heating curves. T_d^{95} and T_{max} are the temperatures for 5% weight loss and the temperature for the maximum decomposition rates, respectively, according to TGA data. Char yield (CY) was measured by TGA

	p_{OH} (%)	M_{NMR} (g mol^{-1})	M_n (g mol^{-1})	M_w (g mol^{-1})	$Đ$	T_g (°C)	T_d^{95} (°C)	T_{max} (°C)	CY (%)
PVA	—		—	—	—	67	267	312	5.4
PI1	59	25 000	—	—	—	93	277	322	11.0
PI2	63	31 000	31 300	76 600	2.4	61	267	316	4.7
PI3	64	40 000	37 700	67 400	1.8	38	264	318	7.0
PI4	72	42 000	38 100	92 000	2.4	56	275	320	5.8
PI5	68	34 000	66 100	167 000	2.5	53	287	320	9.6
PI6	64	39 000	62 800	108 200	1.7	61	277	322	5.4

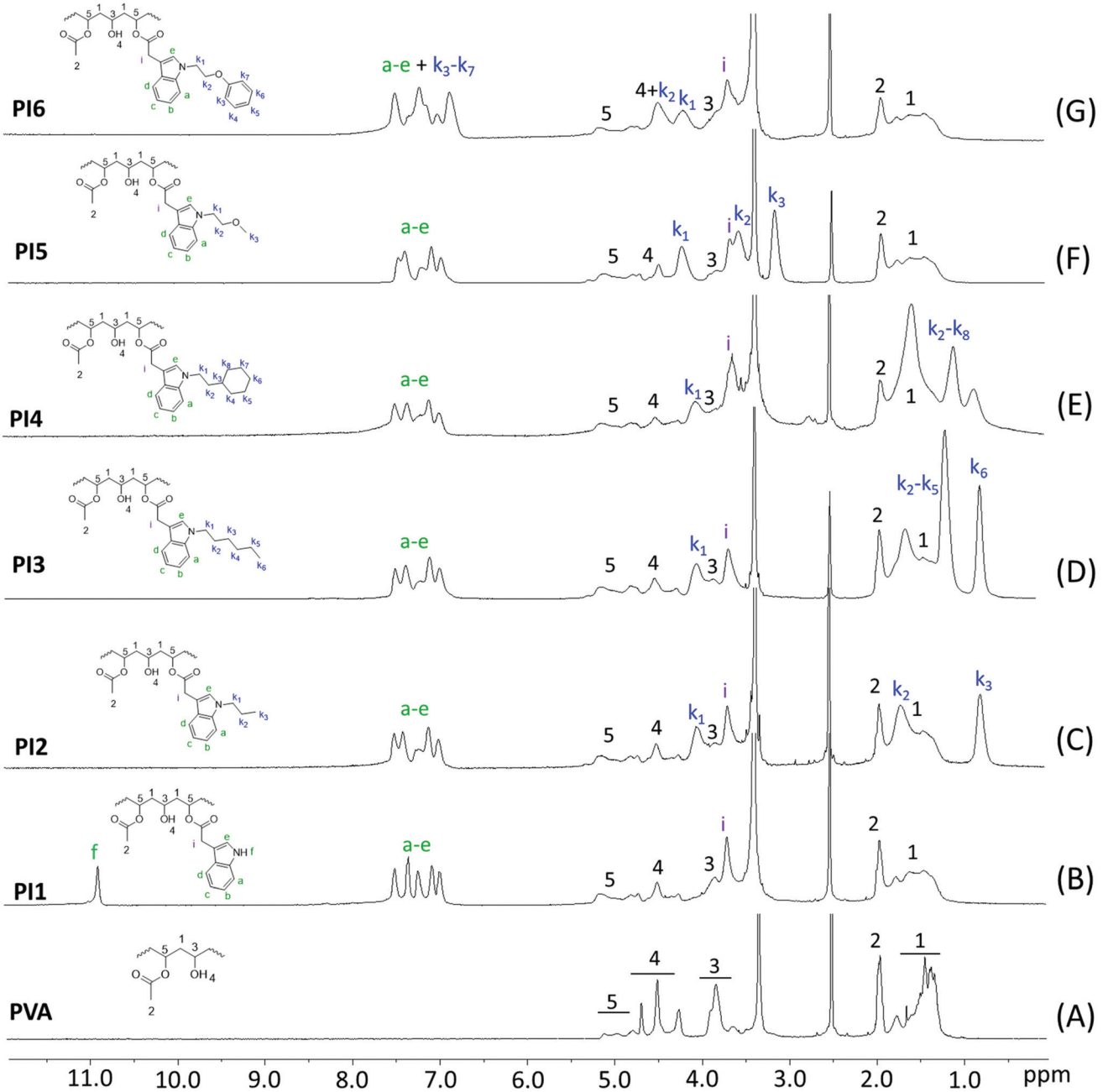

Fig. 1 ^{1}H NMR spectra of (A) initial **PVA** and (B–G) indole-based **PI1–6**, respectively.

protons were observed at 4.73–4.19 ppm (4), containing three discernible signals at 4.69, 4.51, and 4.26 ppm that correspond to *mm*, *mr* and *rr* triads, respectively (Fig. S2, ESI†).[77] The backbone CH_2 signals were observed at 1.85–1.20 ppm (1).

The ^{1}H NMR spectra of **PI1–6** (Fig. 1B–G) showed significantly reduced intensities of the OH (4) and C*H*OH (3) signals and increased intensity of the C*H*OOR signal (5), which confirmed the conversion of OH groups. In addition, new broadened signals appeared in the ^{1}H NMR spectra of **PI1–6**, including the indole aromatic signals (*a–e*) and various *N*-substituted signals (k_1, k_2, k_3, *etc.*), which further confirmed the occurrence of grafting. These new signals were consistent with the peaks for their corresponding grafting agents **1–6** (Fig. S1, ESI†). In addition, the integrals of the OH, methyl, and aromatic signals were compared and used to calculate the p_{OH} values, as discussed earlier. The molecular weight of these polymers (M_{NMR}) was also calculated using the p_{OH} values. For **PI2–4**, these values were quite consistent with the M_n values measured by GPC in chloroform. For **PI5–6**, the calculated M_{NMR} values were lower than the GPC measured M_n values. The differences in the measured values were due to the inherent inaccuracy of the NMR calculations (*e.g.* signal broadening and overlapping)

and GPC measurements (*e.g.* different behavior of the measured polymers and standard polymers in solution). **PI1** was insoluble in chloroform so GPC was not measured.

The chemical structures of **PI1–6** were further characterized by ^{13}C NMR spectroscopy (Fig. S7, ESI†). First, all the signals for the grafting agents **1–6** were unambiguously assigned (Fig. S6, ESI†). The signal observed at ~173.51 ppm (*j*) corresponded to the carbons of COOH groups. In the spectrum of **PVA** (Fig. S7A†), the signals for methyl, methylene, tertiary carbon and carbonyl carbons (signal 1, 2, 3 and 4, respectively) were observed at 21.26, 46.92–44.74, 68.79–63.58 and 170.34 ppm, respectively. After grafting, all the characteristic signals for the **PVA** structures remained discernible (peaks 1–4, Fig. S7B–G, ESI†). In the meantime, a new signal at ~171.35 ppm (4′) appeared in all the ^{13}C NMR spectra of **PI1–6**, which corresponded to the carbonyl carbons with indole units grafted. The COOH carbon signal (*j*) of the grafting agents **1–6** (Fig. S6, ESI†) was not observed in the spectra of the corresponding polymers (**PI1** as an example shown in Fig. 2), indicating the complete removal of the grafting agents. All other characteristic signals corresponding to grafting agents **1–6** were observed in the ^{13}C NMR spectra of all the polymers **PI1–6** (*i.e.* aromatic signals *a–h*, methylene signal *i*, and aliphatic signals k_{1-8}), which confirmed the successful grafting.

Polymers **PI1–6** were further characterized by FTIR spectroscopy (Fig. 3). Before grafting, a broad and strong band centered at 3330 cm^{-1} related to the O–H stretching vibrations with strong hydrogen bonding was observed in the FTIR spectrum of **PVA**. The intensity of this band was dramatically reduced after grafting, which confirmed the reaction of OH groups. However, the strong characteristic ester C=O stretching band (centered at ~1732 cm^{-1}) did not show any noticeable shift after grafting, which was due to the overlapping of the unchanged residual acetate groups of **PVA**. In the meantime, the C–H stretching band at 3000–2800 cm^{-1} was also observed for **PI1–6**, which was due to the overlapping of the C–H stretching of the unchanged **PVA** backbone and the OAc groups. In addition, a new band appeared at 740 cm^{-1} in the FTIR spectra of **PI1–6**, which could be attributed to the out-of-plane bending vibrations of aromatic C–H of the indole ring. Two other new bands at 1589 and 691 cm^{-1} in the spectra of **PI6** corresponded to the vibrations of aromatic C=C and C–H of benzene ring, respectively.

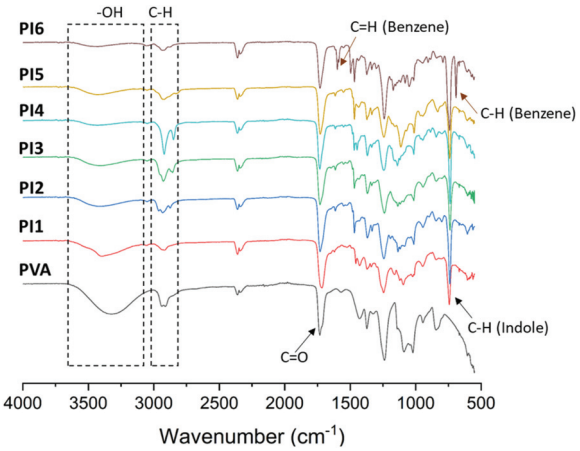

Fig. 3 FTIR spectra of initial **PVA** and indole-based **PI1–6**.

Next, the thermal properties (*e.g.* thermal stability and glass transition temperature) were investigated, because these are related to their processing and manufacturing, which to some extent decide their potential application ranges as biomedical materials. The thermal behavior of the obtained **PI1–6** was evaluated by DSC analyses. According to the second heating DSC curves (Fig. 4), **PI1–6** were all amorphous without any melting endotherm. This was consistent with the results from WAXD measurements (Fig. S8, ESI†), which showed only amorphous halos for **PI1–6** while three sharp diffraction peaks (2θ = 19.5, 22.7 and 40.7°, for crystalline planes ⟨101⟩, ⟨200⟩ and ⟨111⟩) for the initial **PVA**.[78] Furthermore, DSC results also

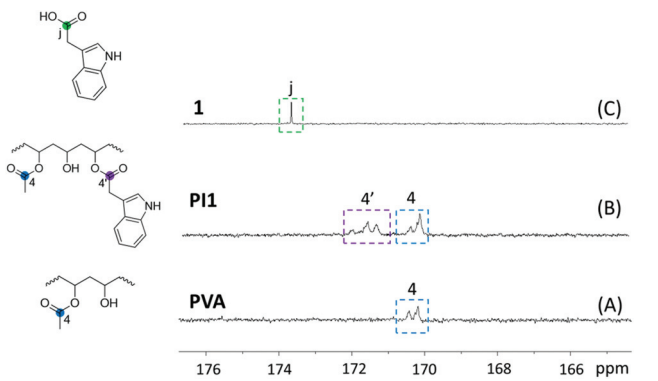

Fig. 2 Zoom-in ^{13}C NMR spectra of (A) initial **PVA**, (B) resulting **PI1** and (C) grafting agent **1** in the carbonyl range (165–176 ppm).

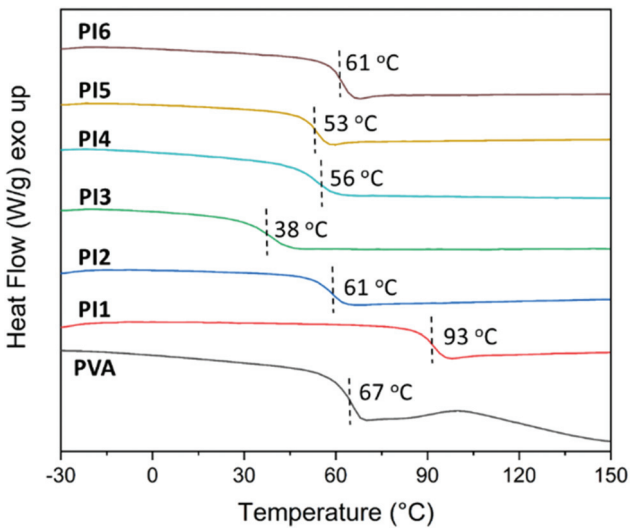

Fig. 4 DSC second heating curves of initial **PVA** and indole-grafted polymers (**PI1–6**).

revealed the glass transition temperatures (T_g) of **PI1–6** in the range of 38–93 °C, depending on the *N*-substituent on indole. **PI1** with unsubstituted indole units showed the highest T_g value (93 °C), which was even higher than that of **PVA** (67 °C). This enhanced T_g was due to the increased bulkiness around the chains (compared to **PVA**) and the preserved ability to form hydrogen bonds (by N–H). **PI2–6** showed lower T_g values than **PVA**, due to the loss of hydrogen bonding forming ability as well as the additional flexibility of alkyl and ether units,[79,80] despite their increased bulkiness compared to **PVA** and **PI1**. Except for **PI3** (T_g ~ 38 °C), other polymers have T_g values ranging from 53–93 °C, which are similar to those of nylon 6/6 (50–60 °C) and poly(vinyl chloride) (65–85 °C). Such T_gs are favourable for plastics toward various commodity applications.

The thermal stability of **PI1–6** was evaluated by TGA measurements (Fig. 5 and Table 1). It was observed that **PVA** presented two decomposition rate maxima (Fig. 5B). According to the literature, the first major decomposition rate maximum at ~312 °C can be attributed to the side chain decomposition, and the second minor decomposition rate maximum at a higher temperature (~428 °C) can be related to the main chain decomposition.[81,82] For **PI1–6**, similar thermal decomposition processes with two rate maxima were observed, which was consistent with the presence of their **PVA** backbones. Compared to their precursor **PVA**, **PI1–6** showed similar or slightly higher T_d^{95} (temperature for 5% mass loss) and T_{max} values (temperature for the maximal rate of weight loss, Fig. 5B, Table 1), as well as higher residual char yields (CY) of **PI1–6**, which could be attributed to the presence of aromatic units.[29,83]

Antibacterial effects

Antibacterial activities of **PI1–6** against six Gram-negative (G−) and three Gram-positive (G+) bacteria were conveniently evaluated according to a disk diffusion method.[29] As presented in Fig. S9,† **PI1–6** all showed larger inhibition zones than the negative control for all the tested bacteria. By analyzing the significance in differences (reflected by the *p* values), most tested polymers showed significantly larger zones of inhibition compared to the negative control (*p* values < 0.05, Table S2, ESI†). The only exception was **PI4**, for which the inhibition zones against two bacteria *Sa* and *Sm* did not show significant difference compared to the negative control (*p* values ≥ 0.05, Table S2, ESI†). This clearly indicates the broad antibacterial properties of indole-based PVAs, regardless of the *N*-substitution.

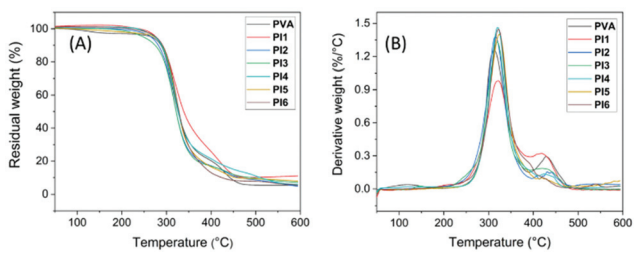

Fig. 5 TGA (A) weight loss and (B) derivative weight loss curves of initial **PVA** and indole-grafted PVAs (**PI1–6**).

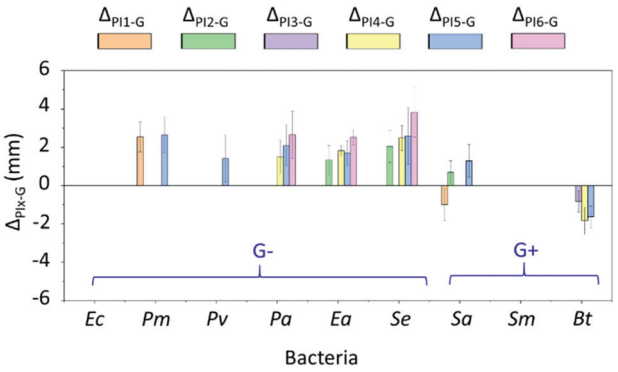

Fig. 6 Difference between the inhibition zones of **PI1–6** and gentamicin (Δ_{PIx-G}, *x* = 1–6). Note, only those Δ_{PIx-G} values with significant differences (*p* values < 0.05, Table S3, ESI†) are shown in the figure. The absence of the data column displayed in the corresponding place means that the inhibition zones of the polymer and gentamicin were comparable without significant difference (*p* values ≥ 0.05, Table S3, ESI†). For instance, for bacteria *Ec* and *Sm* there were no data plotted, which indicated that for these bacteria the effect of the obtained polymers was very similar (no significant difference) to that of gentamicin.

Next, the antibacterial efficiency of **PI1–6** was compared with that of a commonly used small molecular antibiotic, gentamicin (Fig. 6). As a result, **PI1–6** showed generally comparable effects to gentamicin. For most tested bacteria, the zones of inhibition of **PI1–6** and gentamicin did not show significant difference (*p* values ≥ 0.05, Table S3, ESI†). The exceptional cases are shown in Fig. 6 when there was a significant difference in the zones of inhibition of **PI1–6** and gentamicin (Δ_{PIx-G}, *x* = 1–6) reflected by *p* values < 0.05 (Table S3, ESI†). Furthermore, for the six Gram-negative bacteria all **PI1–6** showed either a significantly stronger ($\Delta_{PIx-G} > 0$) or comparable (not shown) antibacterial effect to gentamicin. This indicated the effectiveness of these polymers particularly against Gram-negative bacteria. For the three tested Gram-positive bacteria, the comparison with gentamicin was more complex. For *Sm*, all polymers showed a comparable antibacterial effect to gentamicin. For *Bt*, **PI3–5** showed a significantly lower ($\Delta_{PIx-G} < 0$) antibacterial effect than gentamicin, while that of the other polymers were comparable to gentamicin. For *Sa*, **PI2** and **PI5** showed a significantly better ($\Delta_{PIx-G} > 0$) antibacterial effect than gentamicin, **PI1** showed a significantly lower ($\Delta_{PIx-G} < 0$) antibacterial effect than gentamicin, and the rest of the polymers were comparable to gentamicin. As such a preliminary conclusion is that the obtained polymers were in general comparable to gentamicin against Gram-positive bacteria, while they could be more effective against Gram-negative bacteria.

Next, the impact of *N*-substitution on the antibacterial function of indole-grafted PVAs was investigated. The differences between the zones of inhibition of **PI2–6** with various hydrophobic substituents and **PI1** with N–H units are illustrated

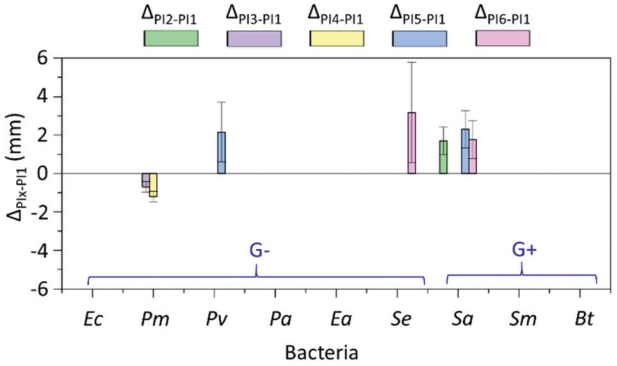

Fig. 7 Investigation on the effect of *N*-substituents. Comparison of the inhibition zones between **PI2–6** and **PI1** ($\Delta_{PIx-PI1}$, x = 2–6). Note, only those $\Delta_{PIx-PI1}$ values with significant differences (p values < 0.05, Table S4, ESI†) were shown. No data displayed means that the inhibition zones between the hydrophobic substituted **PI2–6** and H-substituted (*i.e.* nonsubstituted) **PI1** were comparable without significant difference (p values ≥ 0.05, Table S4, ESI†).

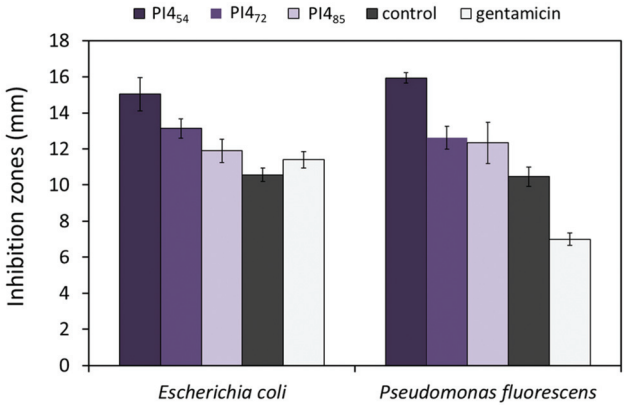

Fig. 8 Inhibition zones of **PI4** samples with different grafting density (conversion of OH groups). The subscript number after **PI4** indicated the OH conversion of the sample. Pure DMF and gentamicin (10 μg per disk) were used as negative and positive controls, respectively. Bacteria: *Escherichia coli* ATCC 8739 and *Pseudomonas fluorescens* (PCL 1701). All experiments were performed in triplicate. The error bars stand for standard deviations.

in Fig. 7. In most cases, the inhibition zones of **PI2–6** were comparable with that of **PI1** without significant differences (p values ≥ 0.05, Table S4, ESI†). This may suggest that neither the indole N–H nor the various hydrophobic substituents were essential in the interactions between the polymers and bacterial membranes. Only on several occasions were the substitution effects observed. For instance, *N*-substituted ether groups (*i.e.* in **PI5–6**) effectively enhanced the antibacterial function against two bacteria (*Pv* and *Sa* for **PI5**, and *Se* and *Sa* for **PI6**). However, *N*-substituted alkyl groups (*i.e.* in **PI2–4**) were less effective. Only *N*-substituted propyl groups (*i.e.* in **PI2**) enhanced the antibacterial function against one bacterium (*Sa*). The presence of larger linear or cyclic alkyl groups (**PI3–4**) showed no enhancement of antibacterial effects against most bacteria and even negative impact in the case of bacterium *Pm*. These observations suggested that ether groups may have a synergistic effect with indole units for the interactions with certain bacterial membranes.[84]

In addition, the possible impact of grafting density (conversion of the OH groups) on the antimicrobial effects for **PI4** was investigated. Two **PI4** samples with lower or higher grafting density were prepared by using 0.5 or 1.5 equivalents of grafting agent **4**. The resulting polymers were characterized by ^{1}H NMR spectroscopy (Fig. S11†), by which their conversion of the OH groups were calculated as 54 and 85%, respectively. Their corresponding molecular weights were also measured by SEC as ~6 and 32 kDa, respectively. The antimicrobial effects of these two new **PI4** samples, namely $\mathbf{PI4_{54}}$ and $\mathbf{PI4_{85}}$ were compared with that of the **PI4** sample synthesized before with 72% OH conversion, namely $\mathbf{PI4_{72}}$. As a result (Fig. 8), all the tested **PI4** samples presented the antibacterial zone of inhibition against the two tested bacteria. In addition, the largest inhibition zones were observed when $\mathbf{PI4_{54}}$ was used against both bacteria. This observed high efficiency of $\mathbf{PI4_{54}}$ could be related to the relatively low molecular weight of the sample (thus high molecular mobility), as well as its relatively large number of unreacted OH groups (thus increased water solubility).

The antibacterial activities of $\mathbf{PI4_{54}}$, $\mathbf{PI4_{72}}$ and $\mathbf{PI4_{85}}$ against two bacteria, *Escherichia coli* ATCC 8739 and *Pseudomonas fluorescens* (PCL 1701), were also evaluated by the standard broth dilution method to determine their minimum inhibitory concentration (MIC) values. After 24 h of incubation at 37 °C of the 96-well microtiter plates, turbidity was noticed in the wells containing ≤12.5 μg mL^{-1} of $\mathbf{PI4_{54}}$, ≤12.5 μg mL^{-1} of $\mathbf{PI4_{72}}$, and ≤25 μg mL^{-1} of $\mathbf{PI4_{85}}$, indicating the growth of bacteria. However, with the concentrations of ≥25 μg mL^{-1} for $\mathbf{PI4_{54}}$, ≥25 μg mL^{-1} for $\mathbf{PI4_{72}}$, and ≥50 μg mL^{-1} for $\mathbf{PI4_{85}}$, no turbidity was observed, indicating the inhibition of bacterial growth. These values were then estimated as close to the MIC values for these polymers (Fig. 9). According to this result, $\mathbf{PI4_{54}}$ showed the most effective bacterial inhibition among the

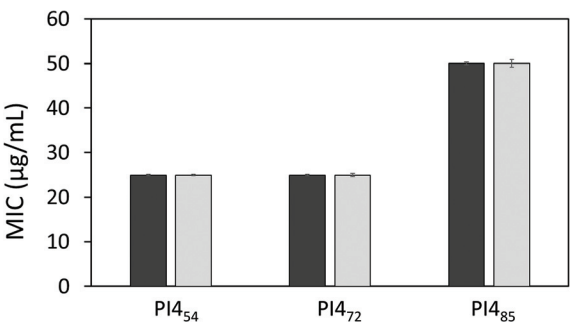

Fig. 9 Minimum inhibition concentrations (μg mL^{-1}) of $\mathbf{PI4_{54}}$, $\mathbf{PI4_{72}}$ and $\mathbf{PI4_{85}}$. The only medium was used as the negative control and only bacterial inoculums were used as a positive control. All experiments were performed in triplicate. Bacteria: *Escherichia coli* ATCC 8739 (dark grey bars) and *Pseudomonas fluorescens* PCL 1701 (light grey bars). The error bars stand for standard deviations.

three **PI4** samples, which was consistent with the disk diffusion results discussed earlier. It should be noted that the water solubility of these nonionic polymers was in general low, which may have an impact on their observed MIC values.

Finally, the anti-quorum sensing (anti-QS) effects of the three **PI4** samples with different OH conversions were investigated by the zone of pigment inhibition that results in an opaque, halo zone of clearance (Fig. S14, ESI†). As shown in Fig. 10, all the three **PI4** samples showed similar anti-QS effects, which were more significant compared to that of gentamicin. Furthermore, it was also noted that the **PI4** sample with the lowest grafting density (*i.e.* $\mathbf{PI4_{54}}$) showed a more significant anti-QS effect for the inhibition of the violacein pigment production of *C. violaceum*. This result preliminarily suggested that these polymers may be potentially interesting targets for further investigations toward materials that resist biofilm formation, which is also regulated by quorum sensing.[85]

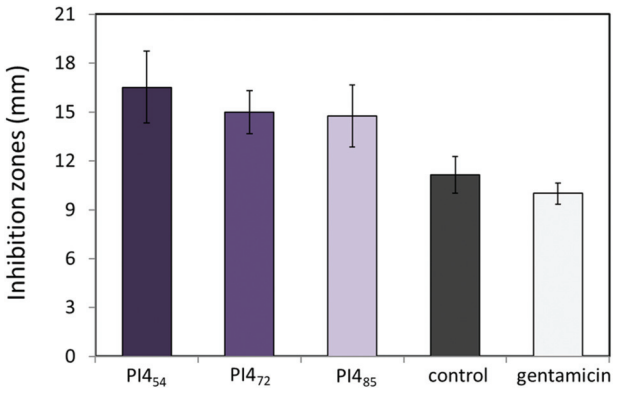

Fig. 10 The anti-QS activity of the three **PI4** samples with different OH conversions ($\mathbf{PI4_{54}}$, $\mathbf{PI4_{72}}$, and $\mathbf{PI4_{85}}$) against *C. violaceum* CV026. Pure DMF and gentamicin (10 μg per disk) were used as negative and positive controls, respectively. All experiments were performed in triplicate. The error bars stand for standard deviations.

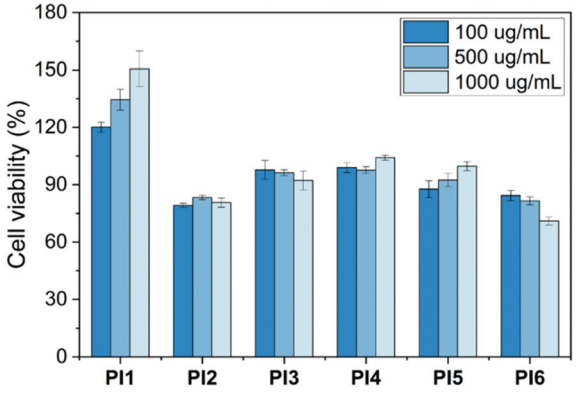

Fig. 11 Cytotoxicity of **PI1–6** at three concentrations (100, 500 and 1000 μg mL^{-1}). Results were presented as relative percent viability of treated cells compared to that of untreated negative control (100% of cell viability, not shown in the graph). The error bars stand for standard deviations.

Cytotoxicity

The cytotoxicity of **PI1–6** to MG-63 osteoblast-like human cells was determined by a standard MTT assay. The results were presented as a relative percentage of the negative control (100% of cell viability). As seen in Fig. 11, less than 30% of reduction of cell viability was observed for all tested polymers during the evaluation period at three different concentrations (10, 100 and 1000 μg mL^{-1}). This indicated that **PI1–6** were non-cytotoxic according to the ISO 10993-5 standard.[86] Furthermore, it was observed that the cell viability increased gradually with the increasing concentration after treatment with **PI1**. This suggested that **PI1** could enhance cell growth and thus might be potentially suitable for various biomedical applications that require promoting cell proliferation (*e.g.* wound healing, tissue engineering and drug delivery),[87–89] which was consistent with other reported polymers (*e.g.* chitosan). To address whether the increasing viability by **PI1** could be related to its interactions with MTT solution, we have performed an additional experiment for **PI1** under the same conditions without adding cells. As shown in Fig. S15 (ESI†), no significant absorbance at 600 nm was observed compared with background at three different concentrations, which demonstrated that **PI1** had no significant interaction with the MTT working solution.

Hemotoxicity

The hemolytic activity of the obtained polymers (**PI1–6**) was evaluated using the HaemoScan Biomaterial Haemolytic Assay (HaemoScan, Netherlands) on human erythrocytes.[76] As shown in Fig. 12, the hemolysis rates of **PI1**, **PI5** and **PI6** were all negligible (<0.01%) after 24 h of contact with red blood cells (RBCs), indicating that these polymers have good hemocompatibility. For the other three polymers (**PI2**, **PI3** and **PI4**), various hemolysis rates were observed (3.4%, 6.9% and 2.9%, respectively). This suggested that the substitutions with alky

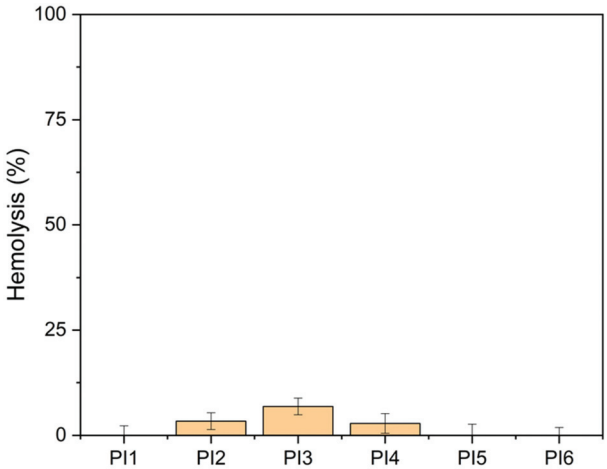

Fig. 12 Hemolytic activity of **PI1–6** (100 μg mL^{-1}). DMSO (1% v/v) was used as the negative control (0% hemolysis). Lysis buffer was used as the positive control (100% hemolysis).

(either linear or cyclic) groups on indole NH could decrease the hemocompatibility of the resulting polymers to some extent, while the substitutions with ether groups have no significant impact on the hemocompatibility, which is consistent with other reported polymers with ether groups.[90,91]

Conclusions

A new series of nonionic indole-based biodegradable poly(vinyl alcohol)s with different *N*-substituents were synthesized, which showed tuneable glass transition temperatures (39–93 °C) and desirable thermal stability. According to the disk diffusion assay, all these polymers showed effective antibacterial function against 9 different human pathogens. In particular, these polymers were generally more effective against the 6 tested Gram-negative bacteria, which were comparable or even superior to the effect of gentamicin. For the 3 tested Gram-positive bacteria, the obtained polymers showed a comparable antibacterial effect to gentamicin, while in some cases significant difference was also noticed. Moreover, we discovered that the antimicrobial function of indole-based PVAs generally did not include significant contribution from the N–H unit or various hydrophobic groups. Only in a few cases the effect of *N*-substitution was observed. This may preliminarily suggest that the antibacterial function of the obtained indole-based PVAs is related to other types of interactions with bacterial membranes (*e.g.* aromatic interactions, or docking on specific membrane proteins) rather than hydrophobic or hydrogen bonding interactions. In addition, we have noticed that the molecular weight and OH conversion had an impact on the antimicrobial and anti-quorum sensing effects of the obtained indole-based PVAs, which suggested that further investigations on molecular design toward optimized molecular sizes and the hydrophobic/hydrophilic balance could provide more valuable information for the development of such a new class of polymer materials. Finally, these obtained polymers showed excellent biocompatibility, particularly for those with ether substituents, which indicated their potential toward various biomedical applications.

Conflicts of interest

There are no conflicts to declare.

Acknowledgements

This work was financially supported by the Mistra Foundation (the "STEPS" project, No. 2016/1489), Swedish Research Council for Sustainable Development (Formas, No. 2021-01107), Carl-Trygger Foundation (No. 18:435), Guangzhou Elite Education Program, and Royal Physiographic Society in Lund. We thank María Del Carmen Casado Muñoz at KTH and Laura Quinn at University College Dublin for the help in supplying the strains *Escherichia coli* ATCC 8739 and *Pseudomonas fluorescens* (PCL 1701), respectively.

Notes and references

1 R. Kurapati, M. Vaidyanathan and A. M. Raichur, *RSC Adv.*, 2016, **6**, 39852–39860.
2 A. Nagaraja, Y. M. Puttaiahgowda, A. Kulal, A. M. Parambil and T. Varadavenkatesan, *Macromol. Res.*, 2019, **27**, 301–309.
3 C. Z. Chen and S. L. Cooper, *Adv. Mater.*, 2000, **12**, 843–846.
4 F. Nederberg, Y. Zhang, J. P. K. Tan, K. Xu, H. Wang, C. Yang, S. Gao, X. D. Guo, K. Fukushima, L. Li, J. L. Hedrick and Y. Y. Yang, *Nat. Chem.*, 2011, **3**, 409–414.
5 A. L. Hook, C. Y. Chang, J. Yang, J. Luckett, A. Cockayne, S. Atkinson, Y. Mei, R. Bayston, D. J. Irvine, R. Langer, D. G. Anderson, P. Williams, M. C. Davies and M. R. Alexander, *Nat. Biotechnol.*, 2012, **30**, 868–875.
6 W. Chin, G. Zhong, Q. Pu, C. Yang, W. Lou, P. F. De Sessions, B. Periaswamy, A. Lee, Z. C. Liang, X. Ding, S. Gao, C. W. Chu, S. Bianco, C. Bao, Y. W. Tong, W. Fan, M. Wu, J. L. Hedrick and Y. Y. Yang, *Nat. Commun.*, 2018, **9**, 1–14.
7 T. Zhu, Y. Sha, J. Yan, P. Pageni, M. A. Rahman, Y. Yan and C. Tang, *Nat. Commun.*, 2018, **9**, 917.
8 M. A. Rahman, M. Bam, E. Luat, M. S. Jui, M. S. Ganewatta, T. Shokfai, M. Nagarkatti, A. W. Decho and C. Tang, *Nat. Commun.*, 2018, **9**, 1–10.
9 A. Kuroki, A. Kengmo Tchoupa, M. Hartlieb, R. Peltier, K. E. S. Locock, M. Unnikrishnan and S. Perrier, *Biomaterials*, 2019, **217**, 119249.
10 E.-R. Kenawy, S. D. Worley and R. Broughton, *Biomacromolecules*, 2007, **8**, 1359–1384.
11 M. R. E. Santos, A. C. Fonseca, P. V. Mendonça, R. Branco, A. C. Serra, P. V. Morais and J. F. J. Coelho, *Materials*, 2016, **9**, 599–632.
12 Z. Zhu, G. Jeong, S. J. Kim, I. Gadwal, Y. Choe, J. Bang, M. K. Oh, A. Khan and J. Rao, *J. Polym. Sci., Part A: Polym. Chem.*, 2018, **56**, 2391–2396.
13 G. N. Tew, R. W. Scott, M. L. Klein and W. F. DeGrado, *Acc. Chem. Res.*, 2010, **43**, 30–39.
14 F. Siedenbiedel and J. C. Tiller, *Polymers*, 2012, **4**, 46–71.
15 I. Banerjee, R. C. Pangule and R. S. Kane, *Adv. Mater.*, 2011, **23**, 690–718.
16 D. Raafat and H. Sahl, *Microb. Biotechnol.*, 2009, **2**, 186–201.
17 G. Li and J. Shen, *J. Appl. Polym. Sci.*, 2000, 676–684.
18 F. Ferrero, M. Periolatto and S. Ferrario, *J. Cleaner Prod.*, 2015, **96**, 244–252.
19 V. W. L. Ng, J. P. K. Tan, J. Leong, Z. X. Voo, J. L. Hedrick and Y. Y. Yang, *Macromolecules*, 2014, **47**, 1285–1291.
20 N. D. Koromilas, G. C. Lainioti, G. Vasilopoulos, A. Vantarakis and J. K. Kallitsis, *Polym. Chem.*, 2016, **7**, 3562–3575.

21 Y. Jiao, L. Niu, S. Ma, J. Li, F. Tay and J. Chen, *Prog. Polym. Sci.*, 2017, **7**, 53–90.
22 E.-R. Kenawy and Y. R. Abdel-Fattah, *Macromol. Biosci.*, 2002, **2**, 261–266.
23 R. Costa, J. L. Pereira, J. Gomes, F. Gonçalves, D. Hunkeler and M. G. Rasteiro, *Chemosphere*, 2014, **112**, 177–184.
24 K. Lewandowska, *J. Solution Chem.*, 2013, **42**, 1654–1662.
25 K. Izutsu and K. Shigeo, *Phys. Chem. Chem. Phys.*, 2000, **2**, 123–127.
26 Y. T. Hung, L. A. McLandsborough, J. M. Goddard and L. J. Bastarrachea, *LWT–Food Sci. Technol.*, 2018, **97**, 546–554.
27 L. J. Bastarrachea and J. M. Goddard, *Appl. Surf. Sci.*, 2016, **378**, 479–488.
28 L. J. Bastarrachea, A. Denis-Rohr and J. M. Goddard, *Annu. Rev. Food Sci. Technol.*, 2015, **6**, 97–118.
29 C. R. Arza, S. Ilk, D. Demircan and B. Zhang, *Green Chem.*, 2018, **20**, 1238–1249.
30 X. Li, S. Ilk, J. A. Linares-Pasten, Y. Liu, D. B. Raina, D. Demircan and B. Zhang, *Biomacromolecules*, 2021, **22**, 2256–2271.
31 M. G. Ciulla and K. Kumar, *Tetrahedron Lett.*, 2018, **59**, 3223–3233.
32 H. Guo, *Eur. J. Med. Chem.*, 2019, **164**, 678–688.
33 M. Raccach, *J. Food Saf.*, 1984, **6**, 141–170.
34 S. Y. Teow, K. Liew, S. A. Ali, A. S. B. Khoo and S. C. Peh, *J. Trop. Med.*, 2016, **2016**, 1–4.
35 K. Shanmugapriya, H. Kim, P. S. Saravana, B. S. Chun and H. W. Kang, *Colloids Surf., B*, 2018, **172**, 170–179.
36 K. Nakano, T. Chigira, T. Miyafusa, S. Nagatoishi, J. M. M. Caaveiro and K. Tsumoto, *Sci. Rep.*, 2015, **5**, 1–10.
37 S. A. El-Mowafy, K. H. Abd El Galil, S. M. El-Messery and M. I. Shaaban, *Microb. Pathog.*, 2014, **74**, 25–32.
38 A. C. Justino de Araújo, P. R. Freitas, C. Rodrigues dos Santos Barbosa, D. F. Muniz, J. E. Rocha, A. C. Albuquerque da Silva, C. Datiane de Morais Oliveira-Tintino, J. Ribeiro-Filho, L. Everson da Silva, C. Confortin, W. do Amaral, C. Deschamps, J. M. Barbosa-Filho, N. T. Ramos de Lima, S. R. Tintino and H. D. Melo Coutinho, *Food Chem. Toxicol.*, 2020, **136**, 111023.
39 L. Martin, P. Gurnani, J. Zhang, M. Hartlieb, N. R. Cameron, A. M. Eissa and S. Perrier, *Biomacromolecules*, 2019, **20**, 1297–1307.
40 Q. Ma, Y. Qu, X. Zhang, Z. Liu, H. Li, Z. Zhang, J. Wang, W. Shen and J. Zhou, *Sci. Rep.*, 2016, **5**, 17674.
41 Q. Ma, X. Zhang and Y. Qu, *Front. Microbiol.*, 2018, **9**, 2625.
42 R. Wang, P. Vega, Y. Xu, C. Y. Chen and J. Irudayaraj, *J. Biomed. Mater. Res., Part A*, 2018, **106**, 1979–1986.
43 J. Kim and W. Park, *Microbiology*, 2013, **159**, 2616–2625.
44 S. Karpagam and S. Guhanathan, *Prog. Org. Coat.*, 2014, **77**, 1901–1910.
45 M. Boopathy, R. Selvam, S. JohnSanthoshkumar and K. Subramanian, *Polym. Adv. Technol.*, 2017, **28**, 717–727.
46 R. J. Cornell and L. G. Donaruma, *J. Med. Chem.*, 1965, **8**, 388–390.
47 L. Erdmann and K. E. Uhrich, *Biomaterials*, 2000, **21**, 1941–1946.
48 R. Jabara, N. Chronds and K. Robinson, *Catheter. Cardiovasc. Interv.*, 2008, **72**, 186–194.
49 N. Shpaisman, L. Sheihet, J. Bushman, J. Winters and J. Kohn, *Biomacromolecules*, 2012, **13**, 2279–2286.
50 O. Hauenstein, S. Agarwal and A. Greiner, *Nat. Commun.*, 2016, **7**, 1–7.
51 S. Weintraub, T. Shpigel, L. G. Harris, R. Schuster, E. C. Lewis and D. Y. Lewitus, *Polym. Chem.*, 2017, **8**, 4182–4189.
52 M. B. Patel, S. A. Patel, A. Ray and R. M. Patel, *J. Appl. Polym. Sci.*, 2002, **89**, 895–900.
53 D. Demircan and B. Zhang, *Carbohydr. Polym.*, 2017, **157**, 1913–1921.
54 T. Nonaka, Y. Uemura, K. Ohse, K. Jyono and S. Kurihara, *J. Appl. Polym. Sci.*, 1997, **66**, 1621–1630.
55 L. Schnaider, S. Brahmachari, N. W. Schmidt, B. Mensa, S. Shaham-Niv, D. Bychenko, L. Adler-Abramovich, L. J. W. Shimon, S. Kolusheva, W. F. Degrado and E. Gazit, *Nat. Commun.*, 2017, **8**, 1–10.
56 B. Zhang, Q. Yu, G. Yan, H. Zhu, X. Y. Xu and L. Zhu, *Sci. Rep.*, 2018, **8**, 1–11.
57 J. Zhang, Y. Chen, Y. Liao, Q. Wang and J. Yu, *Chemosphere*, 2022, **286**, 131551.
58 C. R. Arza, P. Wang, J. Linares-Pastén and B. Zhang, *J. Polym. Sci., Part A: Polym. Chem.*, 2019, **57**, 2314–2323.
59 P. Wang, J. A. Linares-Pastén and B. Zhang, *Biomacromolecules*, 2020, **21**, 1078–1090.
60 P. Wang, C. R. Arza and B. Zhang, *Polym. Chem.*, 2018, **9**, 4706–4710.
61 P. Wang and B. Zhang, *RSC Adv.*, 2021, **11**, 16480–16489.
62 P. Singh, P. Verma, B. Yadav and S. S. Komath, *Bioorg. Med. Chem. Lett.*, 2011, **21**, 3367–3372.
63 N. K. Kaushik, N. Kaushik, P. Attri, N. Kumar, C. H. Kim, A. K. Verma and E. H. Choi, *Molecules*, 2013, **18**, 6620–6662.
64 S. Sathiyaraj, A. Shanavas, K. A. Kumar, A. Sathiyaseelan, J. Senthilselvan, P. T. Kalaichelvan and A. S. Nasar, *Eur. Polym. J.*, 2017, **95**, 216–231.
65 M. Q. Du, Y. Z. Peng, Y. C. Ma, L. Yang, Y. L. Zhou, F. K. Zeng, X. K. Wang, M. L. Song and G. J. Chang, *Chin. J. Polym. Sci.*, 2020, **38**, 187–194.
66 C. Ni, K. Feng, X. Li, H. Zhao and L. Yu, *Prog. Org. Coat.*, 2020, **148**, 105824.
67 M. A. Hassan, A. M. Omer, E. Abbas, W. M. A. Baset and T. M. Tamer, *Sci. Rep.*, 2018, **8**, 1–14.
68 K. E. S. Locock, T. D. Michl, N. Stevens, J. D. Hayball, K. Vasilev, A. Postma, H. J. Griesser, L. Meagher and M. Haeussler, *ACS Macro Lett.*, 2014, **3**, 319–323.
69 A. Srivastava, P. Singh, R. Kumar, S. K. Verma and R. N. Kharwar, *Polym. Int.*, 2013, **62**, 210–218.
70 R. Namivandi-Zangeneh, R. J. Kwan, T. K. Nguyen, J. Yeow, F. L. Byrne, S. H. Oehlers, E. H. H. Wong and C. Boyer, *Polym. Chem.*, 2018, **9**, 1735–1744.

71 V. Sambhy, B. R. Peterson and A. Sen, *Angew. Chem.*, 2008, **120**, 1270–1274.
72 F. Wang, H. Zhou, O. P. Olademehin, S. J. Kim and P. Tao, *ACS Omega*, 2018, **3**, 37–45.
73 S. Ilk, N. Sağlam, M. Özgen and F. Korkusuz, *Int. J. Biol. Macromol.*, 2017, **94**, 653–662.
74 D. Demircan, S. Ilk and B. Zhang, *Biomacromolecules*, 2017, **18**, 3439–3446.
75 CLSI, *Performance Standards for Antimicrobial Susceptibility Testing; Twenty-Second Informational Supplement*, 2022.
76 K. V. Nemani, K. L. Moodie, J. B. Brennick, A. Su and B. Gimi, *Mater. Sci. Eng., C*, 2013, **33**, 4453–4459.
77 T. Congdon, P. Shaw and M. I. Gibson, *Polym. Chem.*, 2015, **6**, 4749–4757.
78 L. Jiang, T. Yang, L. Peng and Y. Dan, *RSC Adv.*, 2015, **5**, 86598–86605.
79 P. I. Tarraco, *J. Polym. Sci., Part A: Polym. Chem.*, 1996, **34**, 925–934.
80 C. Gaina, O. Ursache, V. Gaina and D. Ionita, *Polym.-Plast. Technol. Eng.*, 2012, **51**, 65–70.
81 H. Awada and C. Daneault, *Appl. Sci.*, 2015, **5**, 840–850.
82 L. T. Sin, W. A. W. A. Rahman, A. R. Rahmat and M. Mokhtar, *Carbohydr. Polym.*, 2011, **83**, 303–305.
83 X. L. Wang, T. Fu, D. M. Guo, J. N. Wu, X. L. Wang, L. Chen and Y. Z. Wang, *Polym. Chem.*, 2016, **7**, 1584–1592.
84 K. Fukushima, K. Kishi, K. Saito, K. Takakuwa, S. Hakozaki and S. Yano, *Biomater. Sci.*, 2019, **7**, 2288–2296.
85 V. K. Singh, A. Mishra and B. Jha, *Front. Cell. Infect. Microbiol.*, 2017, **7**, 1–16.
86 I. Standard 11266, *61010-1 © Iec2001*, 2014, **2014**, 13.
87 W. Y. Chuang, T. H. Young, C. H. Yao and W. Y. Chiu, *Biomaterials*, 1999, **20**, 1479–1487.
88 B. Duan, X. Yuan, Y. Zhu, Y. Zhang, X. Li, Y. Zhang and K. Yao, *Eur. Polym. J.*, 2006, **42**, 2013–2022.
89 D. Aggarwal and H. W. T. Matthew, *Acta Biomater.*, 2009, **5**, 1575–1581.
90 K. Fukushima, Y. Inoue, Y. Haga, T. Ota, K. Honda, C. Sato and M. Tanaka, *Biomacromolecules*, 2017, **18**, 3834–3843.
91 X. Li, X. Wang, S. Subramaniyan, Y. Liu, J. Rao and B. Zhang, *Biomacromolecules*, 2022, **23**, 150–162.